PERGAMON

Journal of Atmospheric and Solar-Terrestrial Physics 63 (2001) 431–440

Journal of ATMOSPHERIC AND SOLAR-TERRESTRIAL PHYSICS

www.elsevier.nl/locate/jastp

Modeling of geomagnetic field during magnetic storms and comparison with observations

I.I. Alexeev[a,*], Ya.I. Feldstein[b]

[a] *Institute of Nuclear Physics, Moscow State University, Moscow, Russia*
[b] *Institute of Terrestrial Magnetism, Ionosphere and Radio Wave Propagation of the Russian Academy of Science, Troitsk, Moscow Region, Russia*

Received 15 November 1999; accepted 21 February 2000

Abstract

This paper discusses: (a) development of the dynamic paraboloid magnetospheric field model, (b) application of this model for the evaluation of a variety of magnetospheric current systems and their contribution to the ground magnetic field variations during magnetic storms, (c) investigation of auroral electrojet dynamics and behavior of plasma precipitation boundaries, and (d) usage of the paraboloid magnetospheric field model for revealing relationships between geomagnetic phenomena at low altitudes and the large-scale magnetospheric plasma domains. The model's input parameters are determined by the solar wind plasma velocity and density, the IMF strength and direction, the tail lobe magnetic flux F_∞, and the total energy of ring current particles. The auroral particle precipitation boundaries are determined from, the DMSP particle observations; these boundaries are used to calculate the value of F_∞. The influence of the field-aligned tail, and ring currents on the magnetospheric field structure is studied. It is found that the polar cap area is strongly controlled by the tail current. The paraboloid magnetospheric field model is utilized for the mapping of the auroral electrojet centerlines and boundaries into the magnetosphere. Analysis of the magnetic field variations during magnetic storms shows that the contributions of the ring current, tail current, and the magnetopause currents to the D_{st} variation are approximately equal.

Keywords: Magnetospheric magnetic field model; Magnetosphere

1. Introduction

The Earth's magnetosphere is strongly disturbed during magnetic storms. Storm intervals are interesting for study and are important for the safety of geosynchronous satellites and many other practical needs. However, the average magnetospheric field model usually used for the modeling efforts is too crude for the realistic description of the disturbed magnetosphere.

The magnetospheric magnetic field model developed by Tsyganenko, (1995) is widely used in many studies (see also Tsyganenko and Stern, 1996). The latest version of that model T96 uses the observed D_{st} to parameterize the level of activity in the magnetosphere. This input has replaced the K_p-index used in the previous version T89 of the model. The major limitation of the validity of T96 (as it was noted by the author himself in the program reference manual) is the restriction 20 nT $> D_{st} > -100$ nT. Thus, this model cannot be utilized for strong magnetic storms because it is based on spacecraft data collected over many years but does not include intervals of strong storms. In this database, highly disturbed time intervals occupy a small fraction of the entire time interval covered by the data.

In contrast to the empirical models, the paraboloid model of Alexeev et al. (1996) is a dynamic model of the magnetosphere which is able to reproduce well shorter time scales ($\sim$1 h) in D_{st}. This model has no limitations due to the strength of the storm and, therefore, can be used even for super storms.

* Corresponding author. Tel.: 007-095-939-1036; fax: 007-095-939-3553.

E-mail address: alexeev@dec1.npi.msu.su (I.I. Alexeev).

1364-6826/01/$ - see front matter
PII: S1364-6826(00)00170-X

The paraboloid model of Alexeev et al. (1996) is based on the solution of the Laplace equation inside the magnetopause which is a paraboloid of revolution (see also Alexeev, 1978). As it was pointed out by Alexeev and Shabansky (1972) in the case of the earth's dipole source, the magnetospheric magnetic field can be evaluated that has a vanishing normal component at the magnetopause. Similar problem was solved by Alexeev et al. (1975) for the magnetotail plasma sheet source. A version of the magnetospheric model in which magnetopause was a paraboloid of revolution was constructed by Greene and Miller (1990). The paraboloid modeling technique was described by Stern (1985).

We adopt a version of the paraboloid model of Alexeev et al. (1996) which determines the magnetospheric magnetic field by solar wind plasma as well as magnetospheric plasma dynamics. The magnetospheric dynamics is approximated by a sequence of static models of magnetospheric current systems ("wire" approach) which are driven by input parameters that are varied with time.

Kamide et al. (1998) have presented a common view of many investigators on the problem of magnetic storms. Here we will consider a very important issue that was not discussed by Kamide et al. (1998); this issue concerns the contribution of the tail current sheet magnetic field to the D_{st} variations in the course of a magnetic storm. After Burton et al. (1975), the following formula is used to account for the magnetopause current contribution in the observed D_{st}:

$$D_{st} = DR + DCF - D_{st}(0). \quad (1)$$

Here DR is the pressure corrected D_{st} which describes the symmetric part of the disturbed ring current, DCF is the field of the magnetopause Chapman–Ferraro currents, and $D_{st}(0) = +22$ nT is a constant defined by the DR and DCF fields during magnetically quiet intervals. In the framework of the paraboloid magnetospheric magnetic field model, Alexeev et al. (1992, 1996) have shown that during the main phase of a magnetic storm the magnetotail current field DT (as observed at the Earth's surface) is of the same order as DR. A similar result was obtained by Maltsev et al. (1996), and indeed, the conclusion that "the large magnetic disturbance shows characteristics more of a magnetospheric tail sheet current than of a ring current" was made earlier by Campbell (1973). (Note that the triangulated hypothetical current method used by Campbell (1973) is too rough for numerical estimations.)

Kamide et al. (1998) discussed magnetospheric tail dynamics only in terms of unsteady convection and the associated plasma heating. It is known that the energy transfer and/or energy storage in the magnetotail control the energy budget associated with a geomagnetic storm. For this reason, evaluation of the direct contribution of the tail current magnetic field to the D_{st} variation is very important. If the DT field has roughly the same strength as the DR field during the main phase of a magnetic storm, it is necessary to revise a number of fundamental parameters of the ring current obtained on the basis of ground geomagnetic field variation data. This will require modification of the model of DR dynamics in the course of a magnetic storm. If the DT field is essential in the equation of energy balance, we must recalculate the injection function and the ring current decay parameter. Obviously, the relationships between the different contributors to the total magnetospheric energy should also be revised.

Below, based on the study of two magnetic storms (6–11 February and 23–27 November 1986), we will demonstrate the relationships between the contributions from different sources to the D_{st} variation, using the paraboloid model of the magnetospheric field by Alexeev (1978) and Alexeev et al. (1996). The paraboloid model input is determined by independent data obtained from magnetic observatories and AMPTE/CCE and DMSP F6-F7 satellites (Dremukhina et al., 1999). The model calculations show that the D_{st} variation is not only related to the ring current; in considering contributions to D_{st}, other magnetospheric current systems (in particular, the magnetotail currents and the magnetopause currents) should not be overlooked.

2. Model of the magnetospheric magnetic field during magnetic storms

2.1. Accuracy of the paraboloid model approach to magnetopause configuration

In our study, the magnetopause is represented by a paraboloid of revolution. First, we discuss the accuracy of the paraboloid approach. Fig. 1 (adapted from Kalegaev and Lyutov (2000)) shows a meridional cross section of the paraboloid of revolution and points were a number of spacecraft orbits crossed the magnetopause. These magnetopause crossing points was calculated by Kalegaev and Lyutov (2000) from data collected by Sibeck et al. (1991). Solar magnetospheric coordinates of the crossing points were multiplied by the factor $(p_0/p_{sw})^{1/6}$. It describes a magnetosphere scaling by solar wind dynamic pressure. Here p_0 is the average value calculated for all data set, and p_{sw} is a current dynamic pressure at magnetopause crossing time. All points are placed on the GSM x–ρ plot where $\rho = \sqrt{y^2 + z^2}$. One can see that for $x > -30\ R_E$ distances between the crossings and the paraboloid are typically less than $\sim 3\ R_E$. As seen, a least-squares fit to all empirical points (a thin line) is very close to the meridional cross section of the paraboloid of revolution (a heavy line) (Kalegaev and Lyutov, 2000).

2.2. Magnetospheric magnetic field sources

To better explain our approach, we provide below a short description of the paraboloid magnetospheric field model. Utilizing the paraboloid approach, we can construct a time-dependent model of all known magnetospheric

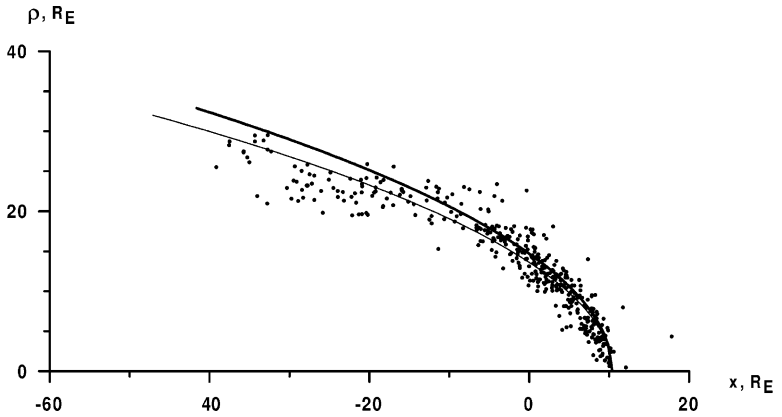

Fig. 1. The two-dimensional cross-section of the magnetopause approximated by the paraboloid of revolution and the points where the satellite orbits crossed the magnetopause determined from measured particles flux and magnetic field vectors. The coordinates of the data points by Sibeck et al. (1991) was corrected by Kalegaev and Lyutov (2000) taken into account solar wind plasma dynamic pressure. Shown are the points in X–ρ plane of GSM coordinates ($\rho = \sqrt{y^2 + z^2}$).

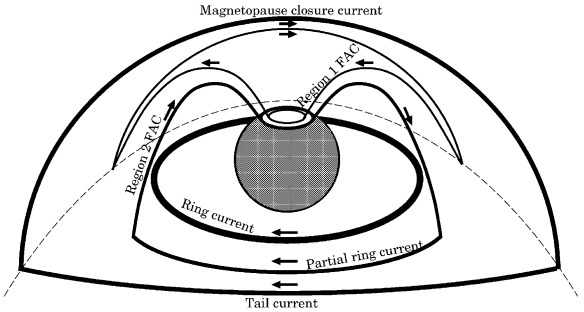

Fig. 2. Current systems used for the calculation of the magnetic field in the magnetosphere. All current systems are closed and one can see the closed currents' loops. If we go from equator (from Earth) to the pole (to the distant tail) we meet: (1) Ring current; (2) Tail current and closure magnetopause current; (3) Partial ring current and Region 2 field-aligned current; and (4) on the day side one can see Region 1 field-aligned currents closed by the magnetopause current.

current systems; however, we note that every current system has its own time scale. The main contributors to the magnetospheric magnetic field are the following (see Fig. 2):

1. The intrinsic geomagnetic (dipole) field, as well as the shielding magnetopause currents, which confine the dipole field inside the magnetosphere (Chapman–Ferraro currents).
2. The tail currents and their closure currents on the magnetopause.
3. The symmetric ring current and the corresponding shielding magnetopause current, whose contributions are mostly important during the magnetic storms.
4. The three-dimensional current systems representing the Regions 1 and 2 field-aligned currents and their closure currents in the ionosphere, in the magnetosphere, and on the magnetopause.
5. IMF penetration into the magnetosphere.

The continuity equations for the magnetic field and the electric current density

$$\operatorname{div} \mathbf{B} = 0 \quad \text{and} \quad \operatorname{div} \mathbf{j} = 0,$$

are true for all the model calculations.

The magnetic field vector $\mathbf{B}_m$ can be calculated by summing the fields of magnetospheric origin

$$\begin{aligned}\mathbf{B}_m(t) = {} & \mathbf{B}_d(\psi) + \mathbf{B}_{cf}(\psi, R_1) + \mathbf{B}_t(\psi, R_1, R_2, F_\infty) \\ & + \mathbf{B}_r(\psi, B_r) + \mathbf{B}_{sr}(\psi, R_1, B_r) \\ & + \mathbf{B}_{fac}(\psi, R_1, F_\infty, I_0) + \mathbf{b}(R_m, \mathbf{B}_{IMF}). \end{aligned} \quad (2)$$

Here $\mathbf{B}_d(\psi)$ is the dipole magnetic field; $\mathbf{B}_{cf}(\psi, R_1)$ is the field of currents on the magnetopause shielding the dipole field; $\mathbf{B}_t(\psi, R_1, R_2, F_\infty)$ is the field of the magnetospheric tail current system (cross-tail currents and closure magnetopause currents); $\mathbf{B}_r(\psi, B_r)$ is the field of the ring current; $\mathbf{B}_{sr}(\psi, R_1, B_r)$ is the field of currents on the magnetopause shielding the ring current field; $\mathbf{B}_{fac}(\psi, R_1, F_\infty, I_0)$ is the field-aligned currents; $\mathbf{b}(R_m, \mathbf{B}_{IMF})$ is the part of the interplanetary magnetic field penetrating into the magnetosphere.

To make the magnetospheric magnetic field (calculated from Eq. (2)) time-dependent, we have to define the time-dependent input parameters: the geomagnetic dipole tilt angle ψ, the geocentric distance to the subsolar point R_1, the geocentric distance to the earthward edge of the magnetospheric tail current sheet R_2, the tail lobe magnetic flux F_∞, the ring current magnetic field strength at the Earth's center B_r, the total strength of the Region 1 field-aligned current I_0, the interplanetary magnetic field vector $\mathbf{B}_{IMF}$, and the magnetic Reynolds number of the solar wind flow R_m which determines the part of the IMF penetrating into the magnetosphere. The ratio of the IMF penetrating into the

magnetosphere to the solar wind IMF was found by Alexeev (1984, 1986) from an analytic solution of the problem of the conducting fluid flowing past paraboloid of revolution.

Modeling of the D_{st} variation was limited to the first five terms on the right-hand side of Eq. (2), because $\mathbf{B}_{fac}$ does not contribute much to the symmetric ground disturbances, and $\mathbf{b}$ is only about 0.1 times the IMF. Therefore, only the limited number of parameters required to specify the above-mentioned current systems has been used. However, it may be possible in principle to determine all contributions by measuring and inputting all the solar wind and magnetospheric parameters.

To calculate the magnetic field disturbances using the paraboloid model, it is necessary to define only five time-dependent input parameters: the geomagnetic dipole tilt angle ψ, the geocentric distance to the subsolar point R_1, the geocentric distance to the earthward edge of the magnetospheric tail current sheet R_2, the tail lobe magnetic flux F_∞, and the ring current magnetic field strength at the Earth's center B_r.

The projection of the geomagnetic dipole tilt angle on the XZ plane of the solar-magnetospheric coordinate system is a known function of UT (e.g. Alexeev et al., 1996). The value R_1 was determined by the dynamic pressure of the solar wind P_{sw} (nPa) and the IMF B_z component (nT) as given by Shue et al. (1997):

$$R_1 = (P_{sw})^{-\frac{1}{6.6}} R_E \begin{cases} 11.4 + 0.013B_z & \text{for } B_z > 0, \\ 11.4 + 0.140B_z & \text{for } B_z < 0. \end{cases} \quad (3)$$

The value B_r was determined by Dessler–Parker–Sckopke relation (Dessler and Parker, 1959; Sckopke, 1966)

$$B_r = B_0 \frac{2K}{3\varepsilon_d}. \quad (4)$$

Here B_0 is the dipole field at the Earth's equator ($\sim$0.3 Gauss=3×10^4 nT), K is the total kinetic energy of the ring current particles, ε_d is the geodipole magnetic field energy above the Earth's surface (Carovillano and Siscoe, 1973). Other input model parameters are determined by the following relationships:

$$R_2 = \frac{R_E}{\sin^2 \theta_n}, \quad F_\infty = 2B_0 \pi R_E^2 \sin^2 \theta_m. \quad (5)$$

Here θ_n is the midnight colatitude of the equatorward boundary of the auroral oval, θ_m is the angular polar cap radius, and R_E is the Earth's radius. In order to obtain the values θ_n and θ_m, we used the DMSP satellite data on the locations of different auroral precipitating particle patterns in the high-latitude region. The K values are calculated from the total ion energy obtained by the AMPTE/CCE satellite inside the radiation belt. The procedure of these model parameters calculation based on the satellite data was described by Dremukhina et al. (1999).

Values of the parameter R_1 where obtained from Shue et al. (1997), but these values were then recalculated by the iteration method using the balance condition between the solar wind dynamic pressure and the paraboloid model magnetic field pressure at the subsolar magnetopause point. These R_1^* values have been used as input parameters for the subsequent calculations of the model's magnetic field variations at the Earth's surface. The difference between R_1 and R_1^* values is small (tenths of R_E). During the periods with southward IMF $R_1^* < R_1$, and $R_1^* > R_1$ during the periods with $B_z \geqslant 0$.

2.2.1. The dipole field and the field of the magnetopause shielding currents

The dipole field $\mathbf{B}_d = -\nabla U_d$, where

$$U_d = \left(\frac{R_E}{R}\right)^3 B_0 (z \cos\psi + x \sin\psi).$$

The magnetic field of the magnetopause shielding currents, $\mathbf{B}_{cf}$, has been calculated by Alexeev and Shabansky (1972). The normal to the magnetopause component B_n of the total field $\mathbf{B} = \mathbf{B}_d + \mathbf{B}_{cf}$ equals zero. The potential U_{cf} ($\mathbf{B}_{cf} = -\nabla U_{cf}$) of the magnetopause shielding currents has been calculated as a solution of the Laplace equation with the boundary condition

$$\mathbf{B} \cdot \mathbf{n} = 0 \quad \text{or} \quad \mathbf{B}_{cf} \cdot \mathbf{n} = -\mathbf{B}_d \cdot \mathbf{n}.$$

Here $\mathbf{n}$ is the normal to the magnetopause.

As a consequence of the paraboloid axial symmetry, the potential U_{cf} has a simple representation in spherical coordinates R, ϑ, ϕ. The polar axis of this coordinate system is the Earth–Sun line, ϑ being the polar angle ($\cos\vartheta = x/R$), and the azimuthal angle ϕ is equal to zero in the X–Z plane of the solar-magnetospheric coordinates. In these coordinates, the scalar potential U_{cf} is written as

$$U_{cf} = -\frac{B_0 R_E^3}{R_1^2} \sum_{n=1}^{\infty} \left(\frac{R}{R_1}\right)^n [d_n^{\parallel} \sin\psi \, P_n(\cos\vartheta) + d_n^{\perp} \cos\psi \cos\phi \, P_n^1(\cos\vartheta)], \quad (6)$$

where

$$P_n(x) = \frac{1}{2^n n!} \frac{d^n (x^2-1)^n}{dx^n} \quad \text{and} \quad P_n^1(x) = \sqrt{1-x^2} \frac{dP_n}{dx}.$$

The first six dimensionless coefficients $d_n^{\parallel}$ and $d_n^{\perp}$ are listed in the second and third columns of Table 1; these coefficients describe the magnetic field of the currents induced on the

Table 1
The coefficients of expansion of the potential U_{cf} in spherical harmonics ($d_n^{\perp}, d_n^{\parallel}$) and in the Bessel functions (D_n, G_n)

n	$d_n^{\perp}$	$d_n^{\parallel}$	D_n	G_n
1	0.6497	0.9403	6.573368	0.670460
2	0.2165	−0.4650	31.07137	2.947181
3	0.0434	0.1293	79.88151	6.039411
4	−0.0008	−0.0148	158.0693	9.771301
5	−0.0049	−0.0160	269.9342	14.04944
6	−0.0022	−0.0225	—	—

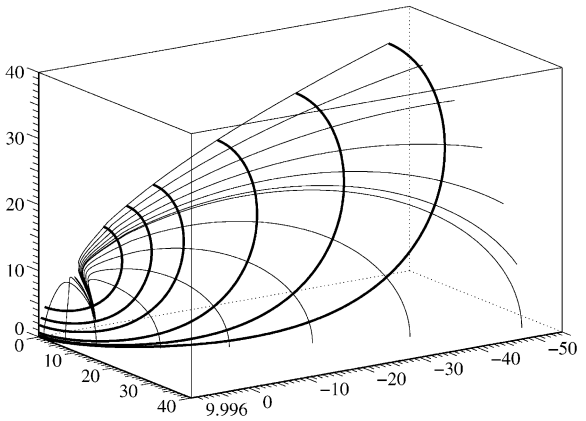

Fig. 3. Chapman–Ferraro magnetopause current which shields the dipole field. The normal (to the magnetopause) component of the total field $\vec{\mathbf{B}}_n = 0$. Outside of the magnetopause, the magnetic field equals zero.

magnetopause by a dipole perpendicular and parallel to the solar wind flow, respectively.

The expansion parameter of (6) is R/R_1, therefore it can be used only up to $R \leqslant R_1$. Over the right-hand side, it is more convenient to represent the sum of potentials $U_d + U_{cf}$ in parabolic coordinates as an expansion in the Bessel functions

$$U_d + U_{cf} = \frac{B_0 R_E^3}{R_1^2} \sum_{n=1}^{\infty} [\sin\psi\, D_n J_0(\lambda_{0n}\beta) e^{\lambda_{0n}} K_0(\lambda_{0n}\alpha) + \cos\psi \cos\phi G_n J_1(\lambda_{1n}\beta) e^{\lambda_{1n}} K_1(\lambda_{1n}\alpha)]. \quad (7)$$

Here the parabolic coordinates α, β, ϕ are defined through the (x, y, z) solar-magnetospheric Cartesian coordinates

$$\beta^2 - \alpha^2 + 1 = 2x/R_1,$$
$$\alpha\beta \sin\phi = y/R_1,$$
$$\alpha\beta \cos\phi = z/R_1. \quad (8)$$

In Eq. (7), λ_{0n}, λ_{1n} are the solutions of the equations $J_0'(x) = 0$ and $J_1'(x) = 0$, respectively. We will use (6) for the case $\alpha < \alpha_0$, and (7) for the case $\alpha > \alpha_0$. The value of α_0 is determined by the distance to the inner edge of the geomagnetic tail current sheet, R_2:

$$\alpha_0 = \sqrt{1 + \frac{2R_2}{R_1}}. \quad (9)$$

In numerical calculations, we used the first six coefficients D_n and G_n, presented in the fourth and fifth columns of Table 1. Fig. 3 shows the magnetopause currents (heavy lines) which shield the dipole field, and the magnetic field lines (thin lines) of the magnetospheric field which go to the magnetopause.

2.2.2. Magnetic fields of the tail current system

We used a model of the tail current system magnetic field which takes into account the finite thickness of the current sheet (Alexeev et al., 1975; Alexeev and Bobrovnikov, 1997). The current sheet is placed at $\alpha > \alpha_0$ and $0 < \beta < \beta_c(\phi)$, where the function $\beta_c(\phi)$ is

$$\beta_c(\phi) = \begin{cases} \dfrac{d}{\alpha_0 R_1 |\cos\phi|} & \text{for } |\cos\phi| \geqslant \dfrac{d}{\alpha_0 R_1}, \\ 1 & \text{for } \dfrac{d}{\alpha_0 R_1} \geqslant |\cos\phi|. \end{cases} \quad (10)$$

Here d is the half thickness of the current sheet. Inside of the current sheet, the magnetic field of the tail current system is a sum of two terms

$$\mathbf{B}_t = \mathbf{B}_2 - b_t R_1 \nabla U_{t1}. \quad (11)$$

Here b_t is the magnetic field strength in the tail lobe at the inner edge of the tail current sheet. This value is defined by the model parameters R_1, R_2, and F_∞:

$$b_t = \frac{2F_\infty}{\pi R_1^2 \alpha_0}. \quad (12)$$

$\mathbf{B}_2$ is found here as a partial solution of the vector potential problem:

$$B_{2\alpha} = b_t \frac{\alpha_0}{\alpha} \frac{\beta}{\beta_c(0)} \frac{\cos\phi}{\sqrt{\alpha^2 + \beta^2}}, \quad B_{2\beta} = 0, \quad B_{2\phi} = 0. \quad (13)$$

The current density vector is proportional to $\nabla \times \mathbf{B}_2$. It is tangential to the paraboloid $\alpha = \text{const}$ and parallel to the equatorial plane. The scalar potential U_{t1} (see Eq. (11)) defines a component of the tail magnetic field which is perpendicular to the equatorial plane. The potential U_{t1} can be written as

$$U_{t1}(\alpha, \beta, \phi) = \sum_{k,n=1}^{\infty} c_{nk} \cos n\phi\, J_n(\lambda_{nk}\beta) K_n(\lambda_{nk}\alpha). \quad (14)$$

Here λ_{nk} is the kth solution of $J_n'(x) = 0$. Outside of the current sheet, the scalar potential U_t of the magnetic field of the tail current system is

$$U_t = b_t R_1 \begin{cases} \displaystyle\sum_{k,n=1}^{\infty} b_{nk} \cos n\phi\, J_n(\lambda_{nk}\beta) I_n(\lambda_{nk}\alpha) \\ \quad \text{for } \alpha < \alpha_0,\ 1 \geqslant \beta > 0, \\ \alpha_0 \ln\alpha\, \text{sign}(\frac{\pi}{2} - |\phi|) + U_{t1}(\alpha, \beta, \phi) \\ \quad \text{for } \alpha \geqslant \alpha_0,\ 1 \geqslant \beta \geqslant \beta_c(\phi). \end{cases} \quad (15)$$

In Eqs. (14) and (15), the coefficients b_{nk} and c_{nk} are defined by f_{nk} as

$$b_{nk} = 2\lambda_{nk} f_{nk} [1 + \lambda_{nk}^2 I_n(\lambda_{nk}\alpha_0) K_n'(\lambda_{nk}\alpha_0)],$$
$$c_{nk} = 2 f_{nk} \lambda_{nk}^3 I_n(\lambda_{nk}\alpha_0) I_n'(\lambda_{nk}\alpha_0)$$

Table 2
Numerical values of the coefficients f_{nk} of scalar potential U_t of the tail current system

k/n	1	3	5	7
1	2.0635	−0.4437	0.2949	−0.280
2	0.108665	−0.053383	0.041799	−0.04171
3	0.029803	−0.017021	0.012939	−0.01203
4	0.012946	−0.008451	0.006415	−0.00537
5	0.006536	−0.004620	0.003708	−0.00309

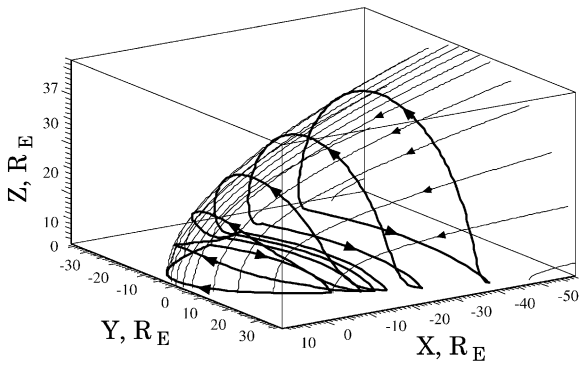

Fig. 4. Tail currents system: shown are the current lines (heavy curves) and the magnetic field lines (thin ones). The normal (to the magnetopause) component of the total field $\vec{\mathbf{B}}_n = 0$. Outside of the magnetopause, the magnetic field equals zero (Alexeev and Bobrovnikov, 1997).

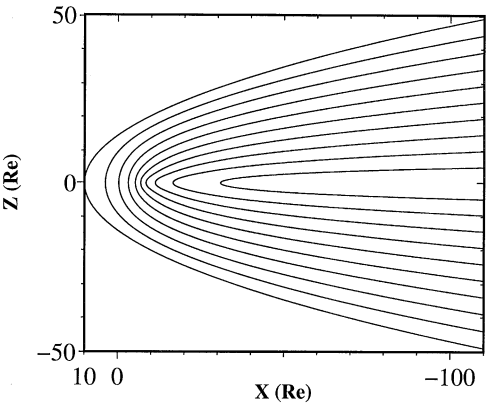

Fig. 5. Field lines of the tail currents system in the noon–midnight meridian plane.

and

$$f_{nk} = \frac{\int_{-\pi}^{\pi} \cos n\phi \{\cos\phi/\beta_c(0) \int_0^{\beta_c(\phi)} J_n(\lambda_{nk}\beta)\beta\,\mathrm{d}\beta + \mathrm{sign}(\pi/2 - |\phi|) \int_{\beta_c(\varphi)}^{1} J_n(\lambda_{nk}\beta)\beta\,\mathrm{d}\beta\}\,\mathrm{d}\varphi}{\pi(\lambda_{nk}^2 - n^2) J_n^2(\lambda_{nk}) I_n'(\lambda_{nk}\alpha_0)}.$$

Numerical values of f_{nk} are presented in Table 2 for $\alpha_0 = \sqrt{2.4}$ (R_2=0.7R_1) and n=2m+1. For $n = 2m$ the coefficients f_{nk} are zero.

Fig. 4 shows current (heavy lines) of the tail current system and the magnetic field lines (thin lines) of this current at the magnetopause for quiet conditions.

The summary field in the magnetosphere $\mathbf{B} = -\nabla(U_d + U_{cf}) + \mathbf{B}_t$ will be determined by the four parameters: ψ, R_1, R_2, F_∞. The last three parameters change with the level of geomagnetic activity, the B_z component of the IMF, and the solar wind plasma dynamic pressure. The mean values of these parameters used in our numerical calculations are $R_1 = 10\,R_E$, $R_2 = 7\,R_E$ and $F_\infty = 380$ *MWb*. These values correspond to $b_t = 40$ nT. Fig. 5 shows the magnetopause and the magnetic field lines of the tail current system in the noon–midnight meridian plane. It is a very important characteristic of the tail current system that the tail currents from the inner part of the tail current sheet are closed at the subsolar magnetopause near noon. The direction of this current at the subsolar magnetopause is opposite to the magnetopause currents that shield the dipole field. Therefore, the subsolar magnetopause distance decreases during the disturbed time for two main reasons: (1) an increase in the solar wind pressure, and (2) a decrease in the magnetospheric field at the subsolar point as a consequence of the increase of the tail current system.

An increase in the density or velocity of the solar wind entails a decrease in R_1. During the strong geomagnetic disturbances, the earthward edge of the tail current sheet moves closer to the Earth (i.e., R_2 decreases), and the size of the polar cap or the value of the tail lobe magnetic flux increases (i.e., F_∞ grows).

2.2.3. *Magnetic field of the ring current*

The ring current is created by trapped energetic particles. Their drift in the geomagnetic field produces a westward azimuthal current. During magnetic storms energetic particles are intensively convected and injected into the inner magnetosphere. The total energy of trapped particles increases and the ring current contribution to the magnetic field at the Earth's surface can reach 1–2% of the dipole field. In the region of the ring current maximum (at $R \simeq 3\,R_E$), its contribution becomes essential. During quiet conditions, the ring current intensity decreases by a factor of 10 or more.

Measurements of the magnetic field during the magnetic storms show strong evidence of significant asymmetry in the ring current, which is especially large during the storm main phase. However, during most of the storm, especially during the recovery phase, the ring current can be treated as axially symmetric. It is convenient to introduce the magnetic field vector potential $\mathbf{A}$ ($\mathbf{B} = \mathrm{curl}\ \mathbf{A}$). The external boundary, where the current becomes zero, coincides with the

distance to the inner edge of the geomagnetic tail current sheet, R_2 ($R_2 \simeq 7\,R_E$). The distance to the current maximum is equal to $0.5\,R_2$.

In spherical coordinates (where the polar axis is anti-parallel to the dipole moment vector and the azimuthal angle is zero at magnetic local noon), the ring current density vector has only one non-zero component $-j_\varphi(R,\theta,\varphi)$. The radial and latitudinal components of the current density are zero. The dependence of the azimuthal current density on the geocentric distance R and on the distance above the equatorial plane $z = R\cos\theta$ is given by the formula

$$j_\varphi = \frac{15 g_R}{2\mu_0} R_2^2 R \sin\theta \begin{cases} R_{rc}^{-7} & \text{for } 0 \leqslant R \leqslant R_2, \\ 0 & \text{for } R > R_2, \end{cases} \tag{16}$$

where $R_{rc}(R) = \sqrt{R^2 + R_2^2}/\sqrt{2}$, and g_R is the magnetic moment of the ring current. The azimuthal component of the vector potential A_φ is written as

$$A_\varphi = g_R R \sin\theta \begin{cases} \dfrac{2}{R_{rc}^3} - \dfrac{1}{R_2^3} & \text{for } 0 \leqslant R \leqslant R_2, \\ \dfrac{1}{R^3} & \text{for } R > R_2. \end{cases} \tag{17}$$

The ring current magnetic field vector $\mathbf{B}_r$ is written as

$$\mathbf{B}_r = \frac{g_R}{M_E} \begin{cases} \left(\dfrac{R}{R_{rc}}\right)^5 \mathbf{B}_d + 2B_0 \left(\dfrac{R_E}{R_2}\right)^3 \left[\left(\dfrac{R_2}{R_{rc}}\right)^5 - 1\right] \mathbf{e}_z \\ \quad \text{for } 0 \leqslant R \leqslant R_2, \\ \mathbf{B}_d \\ \quad \text{for } R > R_2. \end{cases} \tag{18}$$

In (18), $\mathbf{B}_d$ is the Earth's dipole field, $M_E = B_0 R_E^3$ is the Earth's dipole moment, and $\mathbf{e}_z$ is a unit vector along the Z-axis. The strength of the ring current magnetic field at the Earth's center (approximately equal to the surface field perturbation) can be calculated as

$$B_r = |\mathbf{B}_r(0)| = \frac{2 g_R}{R_2^3}(1 - 4\sqrt{2}). \tag{19}$$

This value B_r defines the total energy of ring current particles (see Eq. (4)). The ring current magnetic moment g_R and the total ring current value I as functions of B_r and R_2 are

$$g_R = 0.1 M_E \frac{B_r}{100\text{ nT}} \left(\frac{R_2}{7\,R_E}\right)^3$$

and

$$I = 5.34\text{ MA} \frac{B_r}{100\text{ nT}} \frac{R_2}{7\,R_E}. \tag{20}$$

Fig. 6 shows the magnetic field lines in the noon–midnight meridian plane. These field lines show the magnetic field of the ring currents and of the magnetopause currents that shield the ring current field.

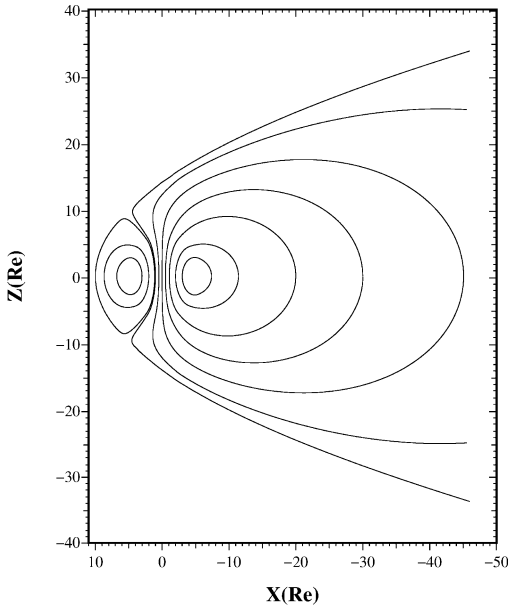

Fig. 6. Ring current system: shown are the magnetic field lines of the ring current and the shielding current. The normal (to the magnetopause) component of the total field $\vec{\mathbf{B}}_n = 0$. Outside of the magnetopause, the magnetic field equals zero.

3. Magnetic storms of 23--27 November 1986

The paraboloid magnetospheric field model allows us to calculate contributions of a number of magnetospheric current systems to the D_{st} variation during magnetic storms.

Fig. 7a shows contributions to the ground geomagnetic variations from the geotail current system, B_t, the Chapman–Ferraro currents, B_{cf}, and the ring current field, B_r during the magnetic storm of 23–27 November, 1986 (Dremukhina et al., 1999). Here the magnetic field of the induced currents inside the Earth has also been taken into account by multiplying factor 1.5 of the model horizontal perturbation field. The estimation of this factor by Langel and Estes (1985) gave 1.3 because the Earth is not perfectly diamagnetic. But we use 1.5 for excluding of undefinity connected with Earth's conductivity. Values of B_r have been calculated based on the values of the total ion energy measured by the AMPTE/CCE satellite (Dremukhina et al., 1999). As one can see, values of B_{cf}, B_r and B_t have comparable and large values during the main phase of the storm. The time behaviors of B_{cf} and B_t are similar, but the directions of these vector are opposite to each other. During the recovery phase B_{cf} and B_t decreased faster than B_r.

Fig. 7b shows comparisons between the model's magnetospheric magnetic field $B_m - B_d$ and the D_{st} index. As calculated for the entire storm interval, the correlation coefficient between D_{st} and $B_m - B_d$ is equal to $r = 0.82$, and the standard deviation is $\sigma = 16.1$ nT.

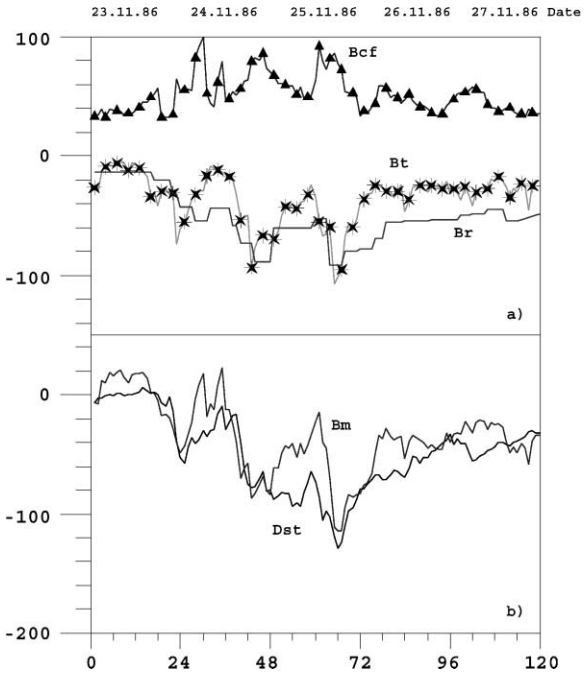

Fig. 7. (a) During the magnetic storms of 23–27 November 1986 the contributions of magnetospheric current systems to the ground D_{st} variations as calculated by using the paraboloid model of the magnetosphere. Triangles — Chapman–Ferraro currents B_{cf}, asterisks — the geotail current system B_t, and solid curve — the ring current field B_r. (b) Comparison of the model field $B_m - B_d = B_{cf} + B_t + B_r$ with the observed D_{st} index.

4. Magnetic storm of 6--11 February, 1986

Kozyra et al. (1998) have pointed out that there is a relatively large discrepancy between the D^*_{st} (where D^*_{st} is the ring current contribution to the disturbance magnetic field D_{st}) inferred from satellite measurements and that estimated from the D_{st} index for storm 6–11 February 1986; neglecting the magnetotail current system can cause such a discrepancy.

Many investigators have studied this storm. Hamilton et al. (1988) estimated the ring current ion energy in the course of this strong magnetic storm with a minimum hourly averaged value of $D_{st} = -300$ nT. Unfortunately, solar wind data are unavailable during the most intense part of the storm main phase, and definitive model calculations of the contributions from the different magnetospheric current systems to D_{st} are impossible.

However, we can compare the observed D_{st} with the total kinetic energy of the ring current ions U_p, obtained from the AMPTE/CCE CHEM observations and presented by Hamilton et al., 1988. In Table 3 (see Hamilton et al. (1988)), U_p is the total kinetic energy of the ring current ions. In the third column, the predicted ΔB (nT) was calculated by using the Dessler–Parker–Sckopke relationship (Dessler and Parker, 1959; Sckopke, 1966); in the fourth column, the observed D_{st} values are listed. In the next two columns of Table 3, the ratios of the predicted D_{st} to the observed D_{st} as calculated by Hamilton et al. (1988) and by Feldstein (1992) are presented. The last column of Table 3 shows the results of our calculations, which include crude estimates of the tail current contribution.

The ratio of the predicted ΔB to the observed D_{st}, given in the 5th column of Table 3 according to Hamilton et al. (1988), varies from 0.24 to 0.84; in all cases, the ratio is less than unity. During the recovery phase (when the ring current might be expected to become more symmetrical), the ratio is close to 0.5. Feldstein (1992) has discussed the reasons for a large discrepancy between the predicted and observed magnetic field values. Feldstein (1992) has corrected the observed values by taking into account the magnetopause current contribution and the effects of the induced currents in the solid Earth. As one can see from the ratios listed in the 6th column, they increase up to about 0.8 during the recovery phase. As we showed in a case study (Alexeev et al., 1996; Dremukhina et al., 1999), the magnetopause current contribution DCF and the tail current contribution DT are approximately equal in magnitude but they have opposite signs. For that approach, the 7th column lists the ratios of predicted ΔB to the observed D_{st}. As one can see, these ratios are close to unity during the recovery phase. Therefore, the relatively large discrepancy between DR inferred from satellite measurements and that estimated from the D_{st} index (observed by Kozyra et al., 1998) disappeared after we took into account the tail current contributions. It is one of the results of our model study that main contributors to D_{st} DR, DT, and $-DCF$ are all of the same order of magnitude. The observed D_{st} variation (storm 6–11 February 1986) corresponds with good accuracy to the symmetric ring current contribution which is determined by the total trapped ion kinetic energy.

5. Tail lobe magnetic field

Let us compare the paraboloid model calculation of the magnetic field with observations in the distant tail. Feldstein et al. (1999) mapped the center, equatorward and poleward boundaries of the eastward and westward electrojets from ionospheric altitudes to the distant magnetotail. The eastward electrojet was mapped to the inner magnetosphere in the ring current region, but the westward electrojet was mapped to the entire plasma sheet, from its inner to its outer boundary. The magnetic field strength B was also determined from the model field. During the magnetic storms of 10 May 1992 ($D_{st} = -200$ nT) and 6 February 1994 ($D_{st} = -120$ nT), mapping of the polar boundary of the westward electrojet to distances near $X = -50\ R_E$ produces a calculated magnetic field strength of 34 nT at 18:36

Table 3
Comparison of ring current ion energy content with observed and predicted onground D_{st} variation

Pass AMPTE/CCE	Total U_p 10^{30} keV for $L = 2$–7	Predicted $\Delta B, nT$	Observed D_{st}, nT	Predicted/observed Hamilton et al. (1988)	Predicted/observed Feldstein (1992)	Predicted/observed
1 in	3.67	−14.6	+0.7	—	—	—
1 out	3.33	−13.2	+2.7	—	—	—
2 in	3.98	−15.9	−7.2	—	—	—
2 out	3.59	−14.3	+1.2	—	—	—
3 in	8.68	−34	−83	0.24	0.33	0.62
3 out	22.1	−88	−88	0.84	0.8	1.5
4 in	12.4	−50	−115	0.31	0.4	0.65
4 out	12.4	−50	−131	0.27	0.3	0.57
5 in	(47.6)	−189	−257	0.68	0.86	1.11
5 out	41.5	−165	−244	0.62	—	1.02
6 in	25.2	−100	−131	0.66	0.88	1.15
6 out	21.8	−87	−133	0.55	0.85	0.98
7 in	17.2	−68	−112	0.49	—	0.91
7 out	16.9	−67	−106	0.50	—	0.94
8 in	14.8	−59	−92	0.49	0.8	0.97
8 out	12.6	−50	−73	0.49	0.72	1.04

UT of 10 May for the first storm and 27 nT at 21:24 UT of 6 February for the second storm. The usual strength of the tail field at these geocentric distances is about 10 nT. The model predicts enhancements of the tail lobe magnetic field several times during the magnetic storm. These results are supported by Geotail data (Kokubun et al., 1996); the data show that the geotail lobe magnetic field strength at geocentric distances ~100 R_E is several tens of nanoteslas during magnetic storms. The tail lobe field increases when the D_{st} variation increases. However, at these distances, the tail lobe field strength varies (with distance) very slowly. For this reason, the agreement between the model calculations and the data is good enough.

6. Conclusion

Studying magnetospheric dynamics in the course of a magnetic storm, we have shown that the tail current contribution to D_{st} is essential. Utilizing the paraboloid model of the magnetosphere, we were able to reproduce short time scale (~1 h) variations in D_{st}. The comparison of the model results with measured D_{st} for the 23–27 November 1986 and 6–11 February 1986 magnetic storms indicates that the tail currents may affect the storm-time D_{st} as much as the ring current. This result is supported by the independent proxy data for the total ring current ion energy estimated from AMPTE/CCE measurements. We use the solar wind data (B_z IMF and dynamic pressure of the plasma flow) as model input. The tail current dynamics has been determined from DMSP particle data. The electron precipitation boundaries were used for the calculation of the polar cap magnetic flux and the midnight equatorial polar oval boundary. These values served for the determination of the tail lobe magnetic flux and the distance to the inner edge of the tail currents.

The tail current dynamics during the studied magnetic storms is strongly supported by geotail observations in the distant tail obtained by Kokubun et al. (1996). Our general conclusion indicates that the depression of the magnetic field strength at the Earth's equator due to the development of the ring current reaches the same value as the tail current magnetic field.

Acknowledgements

The authors acknowledge the members of the NPI MSU and IZMIRAN teams — Elena Belenkaya, Vladimir Kalegaev, Sergey Bobrovnikov, Anatoly Levitin, Ludmila Gromova, and Lidia Dremukhina — who took part in the paraboloid model calculations and the data analysis. The authors also thank Vladimir Papitashvili of the University of Michigan for a careful and helpful review of the manuscript. They thank the referee for useful comments and corrections of the manuscript. The work was supported by the INTAS-RFBR Grant 95-0932. I.I.A. acknowledges partial support from RFBR Grant 98-05-64784 and from the international supplement to NSF Grant ATM-9801941. Y.I.F. acknowledges partial support from the RFBR Grant 99-05-65611 and from the ISSI.

References

Alexeev, I.I., 1978. Regular magnetic field in the Earth's magnetosphere. Geomagnetism and Aeronomy (Engl. Transl.) 18, 447.

Alexeev, I.I., 1984. Normal to magnetopause interplanetary magnetic field component. Geomagnetism and Aeronomy 24 (1), 15 (in Russian).

Alexeev, I.I., 1986. The penetration of interplanetary magnetic and electric fields into the magnetosphere. Journal of Geomagnetism and Geoelectricity 38, 1199.

Alexeev, I.I., Belenkaya, E.S., Kalegaev, V.V., Feldstein, Y.I., Grafe, A., 1996. Magnetic storms and magnetotail currents. Journal of Geophysical Research 101, 7737.

Alexeev, I.I., Bobrovnikov, S.Yu., 1997. Tail current sheet dynamics during substorm. Geomagnetism and Aeronomy 37 (5), 24–31 (in Russian).

Alexeev, I.I., Kalegaev, V.V., Feldstein, Y.I., 1992. Modeling of the magnetic field in a strongly disturbed magnetosphere. Geomagnetism and Aeronomy 32, 8.

Alexeev, I.I., Kirillov, A.A., Chuikova, T.A., 1975. Current system in the tail of the magnetosphere, Geomagnetism and Aeronomy 15, 508–512 (in Russian) (Geomagnetism and Aeronomy (Engl. Transl.) 15, 409, 1976).

Alexeev, I.I., Shabansky, V.P., 1972. A model of a magnetic field in the geomagnetosphere. Planetary Space Science 20, 117.

Burton, R.K., McPherron, R.L., Russell, C.T., 1975. An empirical relationship between interplanetary conditions and D_{st}. Journal of Geophysical Research 80, 4204.

Campbell, W.P., 1973. The field levels near midnight at low and equatorial geomagnetic stations. Journal of Atmospheric and Terrestrial Physics 35, 1127.

Carovillano, R.L., Siscoe, G.L., 1973. Energy and momentum theorems in magnetospheric processes. Reviews of Geophysics and Space Physics 11, 289.

Dessler, A.J., Parker, E.N., 1959. Hydromagnetic theory of geomagnetic storms. Journal of Geophysical Research 64, 2239.

Dremukhina, L.A., Feldstein, Y.I., Alexeev, I.I., Kalegaev, V.V., Greenspan, M., 1999. Structure of the magnetospheric magnetic field during magnetic storms. Journal of Geophysical Research 104, 28,351.

Feldstein, Y.I., 1992. Modeling of the magnetic field of magnetospheric ring current as a function of interplanetary medium parameters. Space Science Reviews 59, 83.

Feldstein, Y.I., Gromova, L.I., Grafe, A., Meng, C.-I., Kalegaev, V.V., Alexeev, I.I., Sumaruk, Y.P., 1999. Dynamics of the auroral electrojets and their mapping to the magnetosphere. Radiation Measurements 30, 579.

Greene, J.M., Miller, R.L., 1990. A model of the magnetosphere. General Atomics Report GA-A20133.

Hamilton, D.C., Gloekez, G., Ipavich, F.M., Studeman, W., Wilken, B., Kzemsez, G., 1988. Ring current development during the great magnetic storm of February 1986. Journal of Geophysical Research 93, 14,343.

Kalegaev, V.V., Lyutov, Yu.G., 2000. The solar wind control of the magnetopause. Advances in Space Research 23 (7-8), 1489.

Kamide, Y., et al., 1998. Current understanding of magnetic storms: storm – substorm relationships. Journal of Geophysical Research 103, 17,705.

Kokubun, S., Fzank, L.A., Hayashi, K., Kamida, Y., Lepping, R.P., Mukai, T., Nakamura, R., Paterson, W.R., Yamamoto, T., Yamoto, K., 1996. Large field events in the distant magnetotail during magnetic storms. Journal of Geomagnetism and Geoelectricity 48, 561.

Kozyra, J.U., Foz, M.C., Sanches, E.R., Evans, D.S., Hamilton, D.C., Nagg, A.F., 1998. The role of precipitation losses in producting the rapid early recovery phase of the Great Magnetic Storm of February 1986. Journal of Geophysical Research 103, 6801.

Langel, R.A., Estes, R.H., 1985. Large-scale, near-field magnetic fields from external sources and corresponding induced internal field. Journal of Geophysical Research 90, 2487.

Maltsev, Y.P., Azykov, A.A., Belova, E.G., Gvozdevsky, B.B., Sadargaleev, V.V., 1996. Magnetic flux redistribution in the storm time magnetosphere. Journal of Geophysical Research 101, 7697.

Sckopke, N., 1966. A general relation between the energy of trapped particles and the disturbance field over the Earth. Journal of Geophysical Research 71, 3125.

Shue, J.-H., Chao, J.K., Fu, H.C., Russel, C.T., Song, P., Khuzana, K.K., Singer, M.J., 1997. A new functional form to study the solar wind control of the magnetopause size and shape. Journal of Geophysical Research 102, 9497.

Sibeck, D.G., Lopez, R.E., Roelof, E.C., 1991. Solar wind control of the magnetopause shape, location, and motion. Journal of Geophysical Research 96, 5489.

Stern, D.P., 1985. Parabolic harmonics in magnetospheric modeling: the main dipole and ring current. Journal of Geophysical Research 90, 10,851.

Tsyganenko, N.A., 1995. Modeling the Earth's magnetospheric magnetic field confined within a realistic magnetopause. Journal of Geophysical Research 100, 5599.

Tsyganenko, N.A., Stern, D.P., 1996. Modeling the global magnetic field the large-scale Birkeland current systems. Journal of Geophysical Research 101, 27,187.